Journal of Materials Chemistry A

Accepted Manuscript

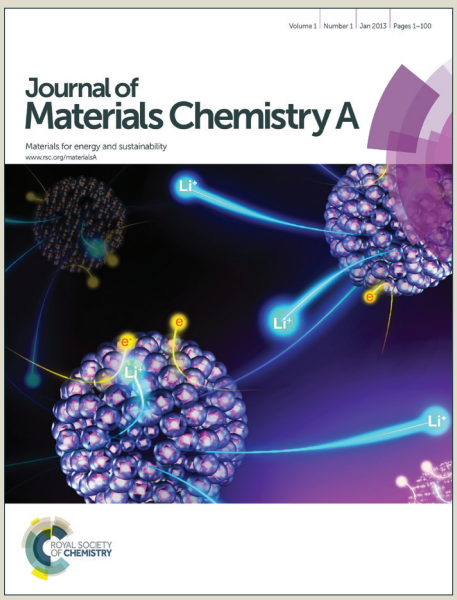

ROYAL SOCIETY OF CHEMISTRY

www.rsc.org/materialsA

Journal Name

RSCPublishing

ARTICLE

Graphene Microsheets from Natural Microcrystalline Graphite Minerals: Scalable Synthesis and Unusual Energy Storage

Cite this: DOI: 10.1039/x0xx00000x

Received 00th January 2012,
Accepted 00th January 2012

DOI: 10.1039/x0xx00000x

www.rsc.org/

Junying Wang,[a] Jianlin Huang,[a] Rui Yan,[a,b] Faxing Wang,[a] Wengang Cheng,[a] Quangui Guo,[a] Junzhong Wang*[a]

Mass production of graphene from graphite at low cost is essential for its practical application since there is huge storage of natural graphite minerals on earth. However, extracting graphite from the minerals usually involves complex and polluted purification process. Here, natural microcrystalline graphite minerals were directly used to produce high-quality graphene microsheets at high yield of > 70% through a scalable electrochemical & mechanical exfoliation approach. The graphene microsheets present the feature of small sheet sizes of 0.2 - 0.6 μm^2 and < 5 atomic layers, low defects and high purity. The graphene microsheets can be highly dispersible in various solvents (the absorption coefficient of graphene microsheets dispersed in isopropanol is around 11.00 cm^{-1}) and printable/paintable to make conductive films with a low sheet resistance of ~10 ohm/squ. The graphene products were used for energy-storage electrodes for supercapacitor and lithium ion battery. The supercapacitor reaches high-rate areal performance of 77 mF/cm^2 area capacity at high charge/discharge rate of 20 mA/cm^2. Notably, graphene anode batteries have high coulombic efficiency of 99.2% and high reversible specific capacity of 390 mAh/g (after 220 cycles) at 40 mA/g and of 200 mAh/g at 595 mA/g for fast charge/discharge time of 17 min. This investigation demonstrates that graphene microsheets can be directly prepared from natural graphite minerals at high yield and low cost and potentially used for high-rate energy storage.

1. Introduction

Mass production of high-quality of graphene at low cost is essential for their practical application in electronics,[1,2] energy-storage devices [3,4] and polymer composites [5]. Graphite as a starting material to produce graphene has been proved to be a good choice for either high quality [6] or high quantity [7-15] of graphene. The current popular chemical Hummers method [7] suffers from the problems of high cost and the treatment of oxidative chemicals (such as concentrated H_2SO_4). On earth there is huge storage of natural graphite minerals including flake graphite and microcrystalline graphite ones. The former mineral usually contain large crystal size of > 10 μm of graphite flakes but a low content of carbon, in contrast, the later usually has small crystal size of < 1 μm but high microcrystalline graphite content of > 60 wt% [15-18]. However, it is usually polluted and costive to extract graphite from natural graphite mine by a multi-step process [16,17]. Moreover, microcrystalline graphite can't be produced from its mineral by conventional floatation separation process for flake graphite production because of the small sizes of graphite [15-17]. In China, highly toxic hydrogen fluoride (HF) was often used to remove silicate and silica components of the minerals to purify microcrystalline graphite at the cost of sacrificing the environment.

Electrochemical exfoliation of graphite to make graphene attracts increasing interests.[9-12] Various electrolytes were used for the electrochemical process at single graphite electrode with the product of different quality and layer number of graphene.[9-12] Few-layer graphene flakes with 1-2 μm sheet size at high yield were realized through lithium salts in propylene carbonate into a graphite negative electrode following strong power sonication.[9] Ion liquid[10] and aqueous solutions[11] were used to produce graphene sheets at the positive electrode with more defects owing to oxidation reaction of graphite/graphene with the electrolyte at high potential positive electrode. Very recently, aqueous solutions (such as 0.1 M $(NH_4)_2SO_4$) were used for electrochemical exfoliation of graphite positive electrode at very high yield while it accompanies with the hydrolysis of water at large current density at high potential of 10V.[12] However, in various electrochemical or liquid exfoliation process, the starting graphite material is usually pure graphite, and natural graphite minerals used to make graphene has not been reported yet.

This work aims at extracting graphene directly from natural microcrystalline graphite minerals without going to the

purification process from graphite minerals to graphite. A scalable approach combining electrochemical and mechanical exfoliation to directly prepare graphene microsheets (GM) from natural microcrystalline graphite minerals (MGM) at high yield was developed. The idea is based on the fact of good electrical conductivity (several ohms) of native MGM minerals and the differences of the density and solubility between graphite and the residue (such as silicates) components of the minerals. Polar carbonate solvent solvated ions of sodium complex cations and perchlorate anions can be pushed to intercalate into graphite during high potential/current charging. Ball milling can shorten the ions transport pathways of charge/discharge by cutting mineral particle sizes and supply with robust shear exfoliation [13,14] to produce graphene at high yield and large scale. In addition, the surface strain of hydrophobic solvated graphite/graphene is different from the hydrophilic impurities of the minerals onto water surface, which supplies with a basis for a new floatation separation process. Our experiments show that the productivity of the 1 - 4 atomic layers of graphene over the graphite in the mineral is > 70%. Furthermore, the graphene products were highly dispersible in various solvents to make conductive inks for painting films. Further, GM prepared can be used for high-rate supercapacitor and lithium ion batteries. Especially, GM anode material of lithium ion battery reached good cyclability with 99.1% of coulombic efficiency within 17 min charge/ discharge time.

2. Experimental Section

Chemicals and Materials**.** Natural microcrystalline graphite minerals were gifted from Chenzhou Top Graphite Company Limited in Hunan province and from a graphite mountain in Neimeng province, respectively. The following chemicals were obtained from Sinopharm Chemical Reagent and used without further purification: sodium perchlorate ($NaClO_4$ powder, 98%, weight percentage), propylene carbonate (PC, anhydrous, 99.7%), N-Methyl-2-pyrrolidone (NMP, 99%) N,N-dimethylformamide (DMF, 98%), sodium hydroxide (NaOH, 95%), hydrogen chloride (37%).

Natural microcrystalline graphite minerals (MGM) were crashed and wet grounded by a ball miller for 2 hours. For the wet balling, usually the volume ratio of MGM and liquid is around 3/1 and the liquid is the electrolyte of 100 g/L of $NaClO_4$ in propylene carbonate. The fine MGM (~40 g) was then transferred into porous polypropylene bags (1 μm pore sizes) inset carbon rods or flexible graphite foils as electrical contact. The space between the bags is around 1 cm. High potential of ±10 V with direct current was applied to the electrolytic system of 100 g/L of $NaClO_4$ in propylene carbonate. After fully charge/discharge for 48 hours (exchange current direction twice each 8 hours), the graphite mineral mixture was wet milled once more for 2 hours. After that, the mixture was put into water surface in big vessel. The graphene floated onto water surface was collected while the impurity residue precipitated down was discarded. The graphene washed by 1 M NaOH and 0.1 M HCl aqueous solutions and deionized water in turn with the assist of bath sonication.

The graphene microsheets powder was mixed with 5 wt% of poly(tetrafluoroethylene) (60 wt% aqueous suspension) to form the electrodes of a supercapacitor. The electrodes were pasted and pressed to a dense film onto Nickel foam with an active area of 1×1 cm and dried in an oven at 100 ºC for 24 h. The mass loading on one electrode was 0.5 - 5.0 mg/cm^2. The supercapacitors were assembled in a nearly symmetrical two electrodes of graphene pressed onto nickel foams inset by a porous separator (Celgard 3501). 6.0 M of KOH aqueous electrolyte was dropped onto supercapacitors. Cyclic voltammetry, galvanostatic charge/discharge, and electrochemical impedance spectroscopy were carried out on a test cell were performed in CHI 660E.

All electrochemical measurements were performed at room temperature in two-electrode 2016 coin-type half-cells. The GM powder was used as anodes in lithium-ion half-cells. Briefly, about 90 mg of GM active material, 10 mg of poly (vinylidenefluoride) (PVDF) binder and appropriate amount of N-methylpyrrolidone (NMP, the liquid and binder's solvent) were mixed by hand for 30 minutes, then the resulting slurry was spread on Cu foil uniformly using a 100 μm notch bar and dried in a vacuum oven at 120 ºC for 12 h. 0.9 cm of disk-shaped electrodes were punched from the thread using a sacrificial layer of weigh paper to prevent burrs on the disk edges. The electrodes were degassed inside an Ar-filled glove box (< 1 ppm. of oxygen and water, Mikrouna Inc., China) for at least 4 hours and were not exposed to air prior to their assembly into cells. CR 2016 stainless steel coin-type cells were fabricated to evaluate the electrochemical performance for the anodes. The electrolyte was 1 M $LiPF_6$ dissolved in a 1:1 volume ratio mixture of ethylene carbonate (EC) and diethylene carbonate (DEC). A few drops of electrolyte were deposited over the anodes. A Celgard 2400 separator membrane (25 μm thick) was then added, followed by lithium metal foil (99.9%, Alfa Aesar) as the counter electrode. Galvanostatic charge-discharging cycling was performed under different current densities within the voltage range of 0.005 - 3.0 V using a LANHE-CT2001A battery test system (Wuhan LAND electronics Co., Ltd). The cyclic voltammetry experiments were conducted using an Autolab instrument of PGSTAT204 in the potential window of 0.005 to 1.2 V versus Li/Li$^+$.

3. Results and Discussion

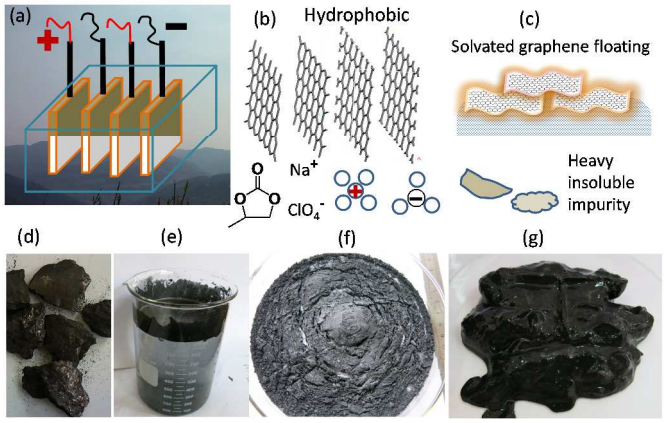

Fig. 1 The preparation of graphene microsheets (GM) using natural graphite minerals as a starting material. (a-c) schematic illustration of (a) graphite minerals electrodes array in charge/discharge cells, (b) electrochemical intercalation of polar solvated ions/electrolyte into graphite (followed mechanical milling), (c) floating separation of GM solvated by hydrophobic organic carbonate electrolyte and heavy impurities in the minerals. (d-g) photographs of (d) natural microcrystalline graphite mineral (MGM) from Hunan province in China, (e) floatation separation of hydrophobic-carbonate

solvated GM floating onto water surface and impurities precipitated down in water. (f,g) graphene microsheets products: (f) freeze-drying powders, (g) conductive inks.

Electrochemical exfoliation of graphite mineral milled was performed in an electrolyte of 100 g/L of $NaClO_4$ in propylene carbonate using MGM fine powder inset carbon rods as both the working electrode and the counter electrode, as shown in Fig. 1a. Before charging, MGM (Fig. 1d and Fig. S2a) were crashed and wet grounded by a ball miller. The fine MGM were then transferred into two pieces of porous polypropylene bags with ~1 μm pore sizes. High potential of ±10 V with direct current was applied to the electrolytic system. During the charge process, perchlorate anions and solvated perchlorate ions can be intercalated into graphite positive electrodes. But sodium ions can not be intercalated into graphite interlayers at the positive electrode (cathode) since XRD analysis shows little difference of graphite cathode before and after charging. Later exchanging the current direction, solvated sodium cations and perchlorate anions can be intercalated into expanded graphite electrodes (Fig. 1b). After fully charge/discharge, the graphite mineral mixture was wet milled once more. After that, the mixture was slowly put into water surface. As illustrated in Fig. 1c and shown in Fig. 1e, graphene microsheets (GM) solvated by hydrophobic carbonate solvents were floating onto water surface while the impurity residue was precipitated down due to the density and surface strain differences between the solvated graphene and silicate/silica residues. After washing and filtering, 25 - 35 g of GM powder could be collected using MGM electrodes (40 g) charging system. Usually, the total yield of GM (either dry powder or/and aqueous inks, Fig. 1f and 1 g) over graphite in MGM can be > 90%.

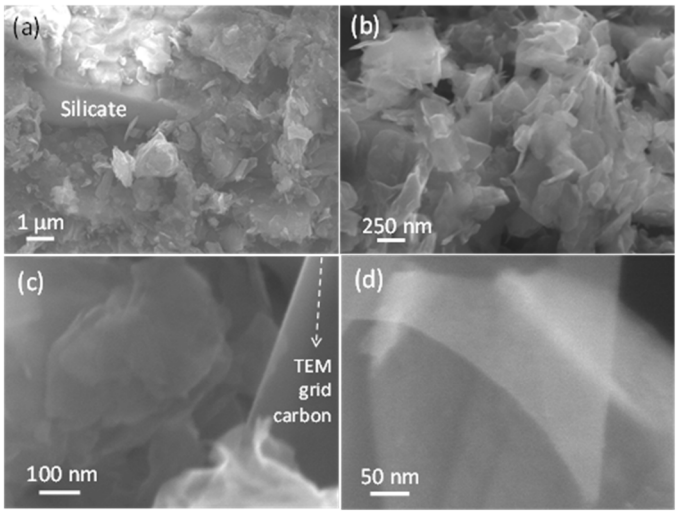

Fig. 2 SEM images of (b-d) graphene microsheets product compared with (a) microcrystalline graphite mineral precursor. (b) narrow size distribution of 0.2-0.6 μm. (c) GM looks thinner than the amorphous carbon support (~3 nm thickness) of TEM grids. (d) High resolution (×200,000) of SEM image shows conductive thin GM.

The purity and morphology of GM product compared with MGM precursor was analysed by elemental analysis, scanning electron microscopy (SEM) with energy dispersive X-ray spectrometry (EDS), as shown in Fig. 2 and Fig. S3-7. The exfoliated GM and graphite phase in MGM could be clearly imaged by SEM without the charging problem of insulating silicate/silica impurity (Fig. 2 and Fig. S3). High resolution SEM images indicate of good conductivity and thinness of <3 nm of GM (Fig. 2c,d). Elemental analysis showed that the carbon content of MGM precursor from Hunan province is around 80-90 wt% and 10-20 wt% other elements such as Al, Si and O (silicate/silica). The carbon content of GM product significantly increases to 97-99 wt%. Examples of EDS analysis onto small areas for the mineral and GM products are shown in Fig. S4,5 and Fig.S7,8, respectively. Thermogravimetric analysis (TGA) data in air presented that the residues of GM and MGM after heating at 1000 °C in air is 10.1 wt% and 1.0 wt%, respectively (Fig. 3a) (as the carbon element was burned in air into gases), which confirmed the elemental analysis and EDS analysis results that significant improvement of the impurity of GM product over MGM precursor. FTIR data revealed that little chemical groups detected (Fig. 3b), which may also indicate of good purity and low defects of the GM. X-ray photoelectron spectroscopy (XPS) was further used to probe the chemical compositions of graphite mineral precursor and GM product. The graphene showed approximately 1.0 atom % oxygen content (Fig. 3c), which is significant lower than that of mineral (16.8 atom % oxygen) and reduced graphene oxide [3,8]. The significant decrease of oxygen contents of graphene product over graphite mineral is owing to the removal of the impurity phases of silica and silicate that have rich oxygen elements in the mineral. The XPS spectra of the C 1s peak (Fig. 3d) disclose the little difference of graphene product and MGM precursor, which further confirmed the non-oxidative process of the graphene preparation method.

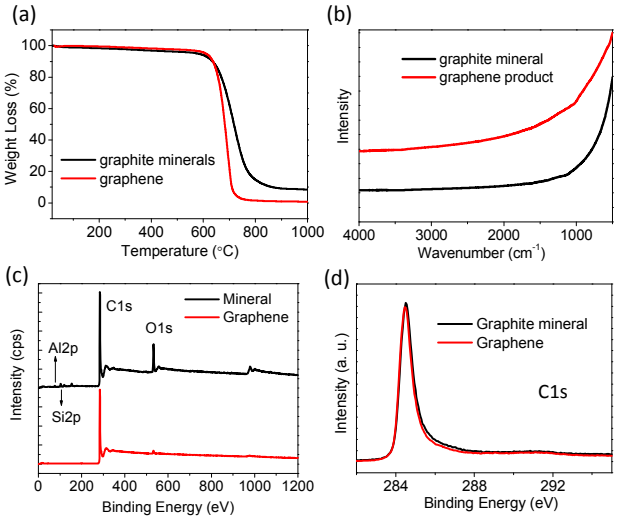

Fig. 3 Spectroscopy characterizations of graphene microsheets (GM) products compared with the mineral MGM precursor. (a) TGA curves in air atmosphere. (b) FTIR spectra. (c,d) X-ray photoelectron spectroscopy (XPS) of spectra of (c) Wide spectra and (d) C1s data.

We further used Raman spectroscopy to identify atomic layers and defects in GM. We performed 488 nm laser line onto GM deposited on SiO_2/Si substrates. The intensity ratio of D

band (1342 cm^{-1}) over G band (1572 cm^{-1}) of GM is 0.27 - 0.35 (Fig. 4a), which is a bit higher than the starting MGM (0.20). However, it is much smaller than for chemically or thermally reduced graphene oxide (~1.1 - 1.5) [8,19] and electrochemically exfoliated graphene in water solution [10]. The defects could probably result from edges increase of GM during exfoliation of MGM. Fig. 4b presents the Lorentzian peak fitting of the 2D peak of GM with < 4 atomic layers compared with graphite.

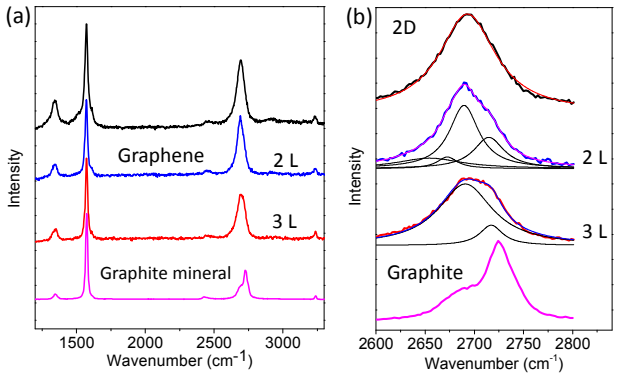

Fig. 4 Raman spectra (488 nm laser) of graphene microsheets. (a) Wide spectra of < 4 atomic layers compared with graphite minerals, (b) Best fit of Lorentzian peak of 2D band.

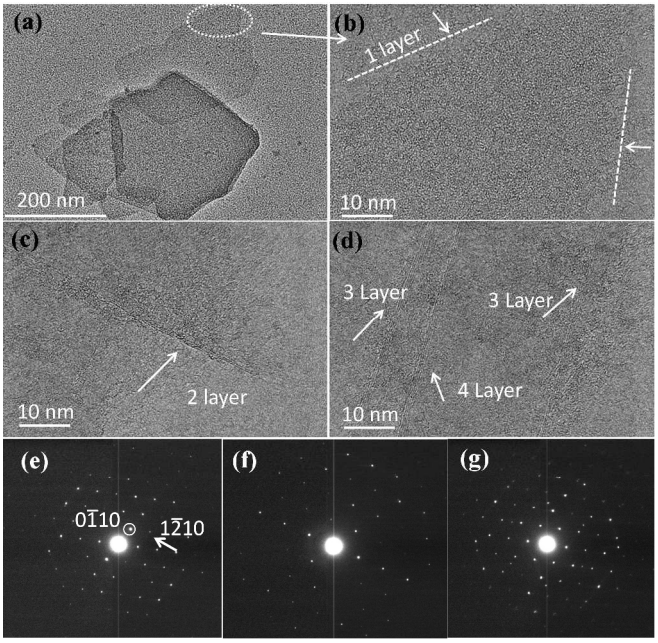

Fig. 5 TEM analysis of graphene microsheets. (a) Low magnification images shows small GM. (b) High resolution image of the graphene part marked in (a): single layer. (b) bilayers, (c) 3 layers and 4 layers, (e-g) typical ED diffraction patterns of 1 - 4 layers.

Analysis of the edges of graphene and the diffraction spot intensity in transmission electron microscopy (TEM) shed some light on the thickness of the graphene layers [14], as shown in Fig. 5 and Fig. S8 and S9. Fig. 5 (b-d) present high resolution TEM images of single layer, bilayer, and 3 - 4 layers, respectively. The average intensity ratio of $\{0\bar{1}10\}$ plane over $\{1\bar{2}10\}$ plane was typically > 1/1, which suggests that the layer thickness was less than five layers. AFM analysis shows the 1.5 nm and 2.6 nm thickness for isolated GM (Fig.S10), which may confirm 2-4 atomic layers. On the basis of statistical analysis of electron microscopy and Raman spectroscopy as well as XRD (002) peak intensity per mass) for the GM, we can conclude that > 70% of the microsheets had the thicknesses of <5 layers (Fig. 6a). This direct exfoliation process can also be applied for graphite minerals with flake graphite that is expandable. Fig. S10 displays the SEM images of MGM with 10% flake graphite in Neimeng province in China and its graphene product with around 10% graphene flakes.

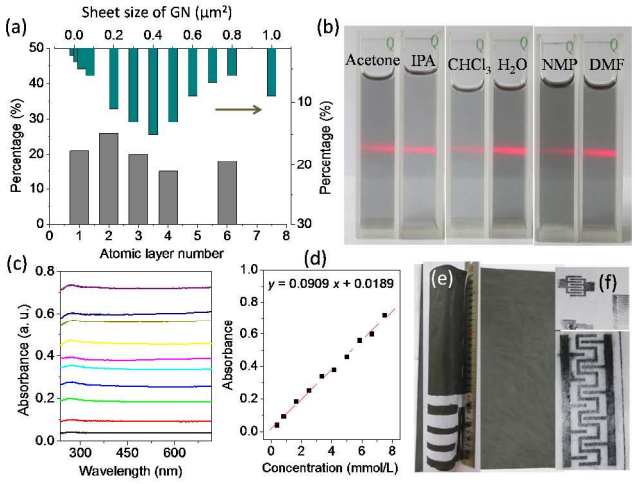

Fig. 6 (a) Thickness and size distribution histograms of the graphene microsheets (GM). (b) Photographs of colloidal GM in various solvents with a red laser line irradiated. (c) UV-visible absorption spectra of graphene dispersions in isopropanol (IPA) ranging from 0.0045 mg/ml to 0.09 mg/ml. (d) The linear relationship of the absorbance at 500 nm and the concentration of the graphene dispersions in IPA. (e) Graphene films painted onto A4 paper by water and IPA dispersions. (f) Graphene pattern onto cotton cloth by screen printing.

Based on the total statistical analysis, the average lateral dimension of the graphene sheets was hundreds of nanometers with a sheet area of 0.2 - 0.6 μm^2, which is comparable to graphite crystal sheet sizes (typical < 1 μm^2) (Fig. 6a). The GM can work like a surfactant and be easily dispersed in acetone, IPA, NMP, DMF, $CHCl_3$ and even H_2O to form colloidal solutions (Fig. 6b and Fig. S2b and S2e). Fig. 6c presented UV-visible absorption spectra of GM in isopropanol with the concentration ranging from 0.0045 mg/ml to 0.09 mg/ml at 298 K. According to the linear relationship of the absorbance at 500 nm and the concentration of GM in IPA (Fig. 6d), the absorption coefficient of graphene microsheets dispersed is calculated as 11.00 cm^{-1}. The GM dispersions in a number of solvents is commonly better than conventional carbon black, which indicated that GM from the natural mineral could potentially replace man-made carbon black as a filler of lots of commercial composites with the advantage of two-dimensional geometry, green process and low cost. Interestingly, the aqueous ink shows colloidal gelation behaviour (Fig. S2e),

which may result from rich HO-edges of small sheet sizes of GM. The simple graphene inks can be painted onto paper and even printed onto cotton cloth, as shown in Fig. 5d and 6e. A sheet resistance of film or lines on A4 paper is as low as ~10 ohm/squ or even below (3.4 ohm for GM powder dried at 80 ºC, as shown in Fig. S2h). The electrical conductivity GM film is comparable to that of high-quality graphene flakes-treated paper [9,12].

A supercapacitor device can be readily made by sandwiching an ion porous separator (Celgard 3501) immersed in 6 M KOH between two nickel foam electrodes coated by GM. The supercapacitor performance was analyzed through both cyclic voltammetry (CV) and galvanostatic charge/discharge experiments and impedance spectroscopy, as shown in Fig. 7. The each electrode of 1 × 1 cm^2 loaded with a mass of around 4 mg preformed relatively high energy density and fast charge/discharge rates. The apparent areal specific capacitance of the thick active graphene film can be reached 99 mF/cm^2 (24.8 F/g) at charge/discharge rate of 1 mA/cm^2 (0.25 A/g). It is 77 mF/cm^2 (19.3 F/g) at even high discharge rate of 20 mA/cm^2 (4 A/g). This is indicative of the formation of an efficient electrochemical double layer and fast ion transport within the graphene electrodes.

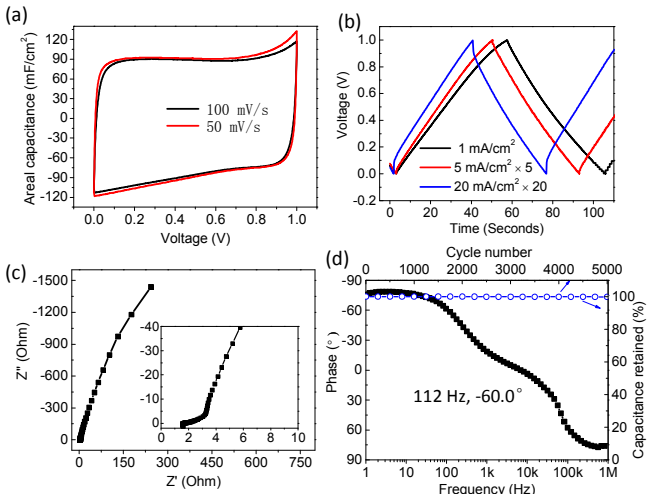

Fig. 7 The performance of supercapacitors of graphene microsheets on nickel foams (6 M KOH electrolyte). (a) Cyclic voltammetry (CV) at a scan rates of 50 mV/s and 100 mV/s. A rectangular CV shape is observed, indicating an efficient double-layer formation. (b) Galvanostatic charge/discharge curves measured at areal current densities of 1, 5 and 20 mA/cm^2 (The x axis is magnified by 5 or 20 times). (c) Nyquist plot showing the imaginary part versus the real part of impedance of graphene film. Inset shows the high-frequency region of the plot. (d) Impedance phase angle versus frequency of graphene film, and capacitance retained with cycling cycle number (Top-X vs Righ-Y).

Electrochemical impedance spectroscopy (EIS) confirmed the high quality of graphene and the fast ion transport within the graphene electrodes. The 1.5 ohm semicircle resulted from electrode contact between metal current collector and active graphene layer (Fig. 7c). By performing impedance measurements for a 200 nm thick graphene electrode, we show that the near -90° phase angle at low frequencies indicates capacitive behavior and 90° phase angles at high frequency indicates inductive behavior [14,20]. And at 120 Hz, the impedance angle of the 200 nm graphene electrode is -60º (Fig. 7d), which is comparable with the capacitor made from vertically oriented GM grown directly on metal current collectors [20,21]. The characteristic frequency f_0 that is corresponding to a phase angle of –45° is 240 Hz for the capacitor (This frequency f_0 marks the point at which the resistive and capacitive impedances are equal [22]). The corresponding time constant t0 (= $1/f_0$) equals 4.2 ms compared with 10 s for the conventional activated carbon capacitor and 1 ms for the aluminum electrolytic capacitor [21].

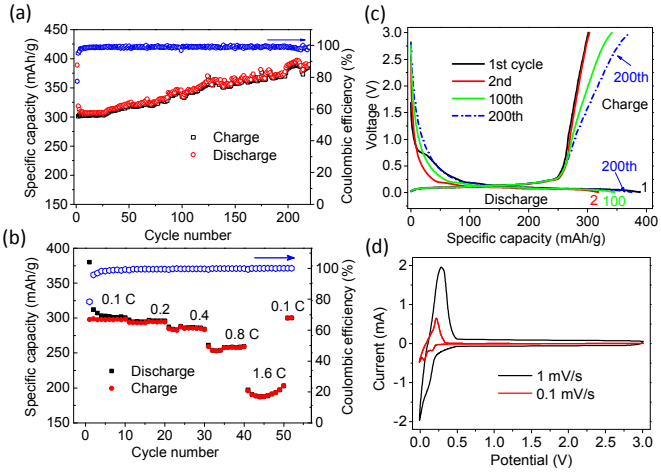

Fig. 8 Electrochemical performances of graphene anode for lithium ion batteries (The graphene loading for the electrodes is around 1.1 mg/cm^2. Lithium metal foil worked as cathode). (a) Specific capacity and coulombic efficiency versus cycle index. The voltage range of charge/discharge is 0.001 V - 3.0 V. (b) Rate capacity and coulombic efficiency versus cycle index. The discharge/charge current density ranges from 40 mA/g (0.1 C) to 595 mA/g (1.6 C). (c) Voltage profiles of the anodic half-cell shows a lithiation–delithiation plateau. (d) The cyclic voltammograms (CV) curves at slow scan rates of 0.1 mV/s and 1 mV/s.

GM product was further used as anode material for lithium ion batteries after it was annealed at 1000 ºC in Ar gas. The batteries were assembled in a Ar glove box using the CR 2016 cell with graphene powder (90 wt% GM and 10% poly (vinylidenefluoride) binder) and lithium metal foil as electrodes, and a 1 M of $LiPF_6$ in a 1:1 (v/v) mixture of ethylene carbonate and diethyl carbonate as an electrolyte. As shown in Fig. 8a, the graphene anode has initial specific capacity of 390 mAh/g, which is higher than the theoretical capacity of graphite (372 mAh/g). Remarkably, a reversible capacity of 390 mAh/g recovered and high average coulombic efficiency of 99.2% (except for the first cycle of 78.6%) at 0.1 C charge/discharge rate (40 mA/g) after 220 cycles has been reached, which demonstrates that the cyclability is significantly better from reduced graphene oxide. A bit more specific capacity of GM than graphite may result from the edge-defects and > 0.34 nm interlayer stacking of small graphene microsheets randomly stacked in variable interlayer distance.[24-27,29,30] Gradually increase with cycling after first cycle may result from the gradual electrolyte wetting and gradual release

of initial capture of lithium of first cycle in dense electrodes of graphene microflakes stacked because of stable solid electrolyte interphase (SEI) formation with cycling. In addition, high coulombic efficiency of 99.1% for rate capacity from 0.1 C to 1.6 C (595 mA/g) was obtained, as shown in Fig. 8b. Notably, 200 mAh/g of specific capacity was retained at high charge/discharge current density of 595 mA/g within 17 min time. This rate-cycability is much better than conventional graphite anode that only < 50 mAh/g can be retained at this current density. The good cyclability of GM anode should be resulted from low-defects of graphene [23-25]. By comparison, the battery performance of graphene anode is better than carbon black (Super P, China) anode. As shown in Fig.S14, first specific capacity of carbon black is 263.6 mAh/g at 37 mA/g with first coulombic efficiency of 47.6% (Fig.S14a). The average coulombic efficiency of 2-40 cycles for rate capacity from 0.1 C to 1.6 C (595 mA/g) is 95.7%.

The flat plateau of lithiation /delithiation of GM is similar to that of graphite and in contrast to that of reduced graphene oxide, which may be relative to the non-oxidation and little defects of GM synthesized. As shown in Fig. 8c, the 200th-cycle voltage profile at < 0.7 V is closer to the 1st one than 100th one, which indicated that stable solid-electrolyte interface (SEI) formed in GM film with cycling can provide stable pathways for Li/Li^+ transport. In contrast, carbon black appeared no plateau of lithiation /delithiation and poor cycling stability (Fig.S14c). The peaks in the low potential of < 0.4 V at a slow scan rate of 0.1 mV/s should be corresponding to insertion /de-insertion of Li into interlayer of few-layer graphene or/and the space of GM stacked [23,24]. When the scan rate increase 10 times, the integrated CV increase 5 times and two peaks at 0.05 V and 0.18 V was changed to single broad peak centered at 0.12 V (Fig. 8d and Fig. S12a and S12b), which could be ascribed to capactive surface-diffusion dominated lithiation/delithiation of GM film (Fig. 7b and Fig. S12c) [23-28]. Our data revealed that low-defective GM stacked has similar capacity and voltage profiles to storage lithium to graphite, which may indicate that there is no big difference for lithium storage mechanism between the GM that can allow the lithium ion insertion/de-insertion into graphene layers stacked and the graphite that can let the intercalation/deintercalation of lithium into its interlayer. In low-defective GM stacked tightly, there exists similar strong π-π interaction between graphene layers and absorption/repulsion for ions of graphite. We think that it is not surprising that the theory that pristine graphene have double theoretical specific capacity of graphite was not realized in our experiments [30, 31]. However, the capacitive diffusion of ions plays more roles for GM than graphite, and high-rate cyclability for battery and supercapacitor was realized. The AC impedance spectrum (Fig. S12) appeared with 4 stages of semicircles may indicate that the charging/discharging process includes SEI formation (largest semicircle), ions/charge transport, lithium accumulation onto GM and lithium intercalation into interlayer of few-layer/multi-layer graphene [29-32], which is different from graphite [32,33], expanded graphite [34], reduced graphene oxide [25,26] or carbon black (Fig.S14)[35]. Precise control of the interlayer distance of graphene layers stacked may provide the insight for energy storage mechanism [23-31].

4. Conclusions

Directly using natural microcrystalline graphite minerals (MGM) as a precursor, a scalable graphene synthesis approach combining electrochemical exfoliation with ball milling was developed. Little oxidative graphene microsheets with high purity can be prepared at high yield of > 70% using the MGM. The graphene products exhibit the feature of low-defects, high crystallinity, small sheet size of hundreds of nanometers and less than 5 layers. The graphene can be well dispersed in various solvents for ink-painting into film or pattern with good electrical conductivity. The graphene powder was successfully used as electrodes for supercapacitor and lithium ion batteries with high-rate electrochemical performance. Especially, graphene anode material for lithium ion batteries performs excellent cycle-ability of high coulombic efficiency ⩾ 99.1% and of reversible specific capacity of 390 mAh/g after 220 cycles and of 200 mAh/g within 17 min charge/discharge time. This cost-effective synthesis approach of graphene from abundant graphite minerals holds the great potential for the commercialization of graphene production.

Acknowledgements

This work was supported by National Natural Science Foundation of China (21373255) and Shanxi Province Science Foundation (2014011016-3) and Hundred Talent Program of Chinese Academy of Sciences (2013SCXQT01).

Notes and references

[a] *Key Laboratory of Carbon Materials, Institute of Coal Chemistry, Chinese Academy of Science,Taiyuan,030001, P R China.*
E-mail: wangjz@sxicc.ac.cn (J.Z. Wang). Tel: 86-351-4040407.
[b] *University of Chinese Academy of Sciences, Beijing 100049, P R China.*

Electronic Supplementary Information (ESI) available: Detailed TEM and SEM images, and EDS analysis for graphite minerals and graphene microsheets, and AC impedance spectra for graphene anode battery. See DOI: 10.1039/b000000x/

References

1 G. Eda, G. Fanchini and M. Chhowalla, *Nat Nanotech.*, 2008, **3**, 270.
2 K. K. Manga, J. Z. Wang, M. Lin, J. Zhang, M. Nesladek, V. Nalla, W. Ji and K .P. Loh, *Adv. Mater.*, 2012, **24**, 1697.
3 M. D. Stoller, S. Park, Y. Zhu, J. An and R. S. Ruoff, *Nano Lett.*, 2008, **8**, 3498.
4 X. Yang, C. Cheng, Y. Wang, L. Qiu and D. Li, *Science*, 2013, **341**, 534.
5 S. Stankovich, D. A. Dikin, G. H. B. Dommett, K. M. Kohlhaas, E. J. Zimney, E. A. Stach, R. D. Piner, S. T. Nguyen and R. S. Ruoff, *Nature*, 2006, **442**, 282.
6 K. S. Novoselov, A. K. Geim, S. V. Morozov, D. Jiang, Y. Zhang, S. V. Dubonos, I. V. Grigorieva and A. A. Firsov, *Science*, 2004, **306**, 666.
7 W. S. Hummers and R. E. Offeman, *J. Am. Chem. Soc.*, 1958, **80**, 1339.
8 S. Park and R. S. Ruoff, *Nat Nanotech.*, 2009, **4**, 217.
9 J. Wang, K. K. Manga, Q. Bao and K. P. Loh, *J. Am. Chem. Soc.*, 2011, **133**, 8888.

10 N. Liu; F., Luo; H., Wu; Y., Liu; C. Zhang; J. Chen, *Adv. Funct. Mater*. 2008, **18**, 1518.
11 C. Y. Su, A. Y. Lu, Y. P. Xu, F. R. Chen, A. N. Khlobystov and L. J. Li, *Acs Nano*, 2011, **5**, 2332.
12 K. Parvez, Z.-S. Wu, R. Li, X. Liu, R. Graf, X. Feng and K. Müllen, *J. Am. Chem. Soc.*, 2014, **136**, 6083.
13 I.-Y. Jeon, Y.-R. Shin, G.-J. Sohn, H.-J. Choi, S.-Y. Bae, J. Mahmood, S.-M. Jung, J.-M. Seo, M.-J. Kim, D. W. Chang, L. Dai and J.-B Baek, *PNAS*, 2012, **109**, 5588.
14 K. R. Paton, E. Varrla, C. Backes, R. J. Smith, U. Khan, A. O'Neill, C. Boland, M. Lotya, O. M. Istrate, P. King, T. Higgins, S. Barwich, P. May, P. Puczkarski, I. Ahmed, M. Moebius, H. Pettersson, E. Long, J. Coelho, S. E. O'Brien, E. K. McGuire, B. M. Sanchez, G. S. Duesberg, N. McEvoy, T. J. Pennycook, C. Downing, A. Crossley, V. Nicolosi and J. N. Coleman, *Nature Mater.*, 2014, **13**, 624.
15 T. Hayashi, K. Saitou, J. Tamura, N. Otsuka and Y. Tonooka, *J. Ceramic Soc. Japan.*, 2000, **108**, 598.
16 X. J. Lu and E. Forssberg, *Minerals Engineering*, 2002, **15**, 755.
17 W. Tang, J-C Kuang, W. Xie, H. Xu, Y-J Deng, C-G Long and B-J Zeng, *Chemical Engineer*., 2012, **26**, 30.
18 Y. F. Li, S. F. Zhu and L. Wang, *New Carbon Mater.*, 2012, **27**, 476.
19 I. K. Moon, J. Lee, R. S. Ruoff and H. Lee, *Nature commun.* 2010, **1**, 1.
20 J. R. Miller, R. A. Outlaw and B. C. Holloway, *Science*, 2010, **329**, 1637.
21 M. F. El-Kady, V. Strong, S. Dubin and R. B. Kaner, *Science* 2012, **335**, 1326.
22 P. L. Taberna, P. Simon and J. F. Fauvarque, *J. Electrochem. Soc.*, 2003, **150**, A292.
23 E. Yoo, J. Kim, E. Hosono, H.-s. Zhou, T. Kudo and I. Honma, *Nano. Lett.*, 2008, **8**, 2277.
24 F. Yao, F. Guenes, T. Huy Quang, S. M. Lee, S. J. Chae, K. Y. Sheem, C. S. Cojocaru, S. S. Xie and Y. H. Lee, *J. Am. Chem. Soc.*, 2012, **134**, 8646.
25 R. Mukherjee, A. V. Thomas, A. Krishnamurthy and N. Koratkar, *Acs Nano.,* 2012, **6**, 7867.
26 P. Guo, H. Song and X. Chen, *Electrochem. Commun*., 2009, **11**, 1320.
27 H. W. Song, N. Li, H. Cui, C. X. Wang, *Nano Energy*, 2014, **4**, 81.
28 A. Kumar, A. L. M. Reddy, A. Mukherjee, M. Dubey, X. Zhan, N. Singh, L. Ci, W. E. Billups, J. Nagurny, G. Mital and P. M. Ajayan, *ACS Nano*, 2011, **5**, 4345.
29. B-M. Goh, Y. Wang, M.V. Reddy, L. Y. Ding, L. Lu, C. Bunker and K. P. Loh, *ACS Appl. Mater. Interfaces,* 2014, **6**, 9835.
30 A. Gerouki, M. A. Goldner, R. B. Goldner, T. E. Haas, T. Y. Liu and S. Slaven, *J. Electrochem. Soc*, 1996, **143**, L262.
31 T. Suzuki, T. Hasegawa, S. R. Mukai and H. Tamon, *Carbon*, 2003, **41**, 1933.
32 D. Aurbach, *J. Power Sources*, 2000, **89**, 206.
33 J. Gnanaraj, S. M. D. Levi, E. Levi, G. Salitra, D. Aurbach, J. E. Fischer and A. Claye, *J. Electrochem. Soc*, 2001, **148**, A525.
34 C. L. Ma, C. Ma, J. Z. Wang, H. Q. Wang, J. L. Shi, Y. Song, Q. G. Guo and L. Liu, *Carbon*, 2014, **72**, 38.
35 K. S. Yun, B. R. Kim, E. Noh, H. J. Jung, H. J. Oh, W. S. Kang, S. C. Jung, S. T. Myung and S. J. Kim, *Jpn. J. Appl. Phys.*, 2009, **52**, 11NM01-1.

A table of contents entry

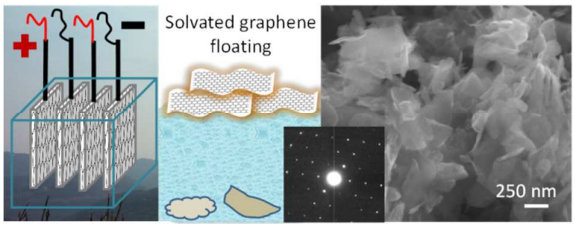

Graphene microsheets, directly produced from natural microcrystalline graphite minerals efficiently, reached 390 mAh/g after 220 cycles as battery anode.